Indian Journal of Chemical Technology
Vol. 31, March 2024, pp. 257-270
DOI: 10.56042/ijct.v31i2.1822

Electro-osmotic effect on the peristaltic flow of Williamson nanofluid through a porous medium in the presence of activation energy and modified Darcy's law

M. M. Abdelmoneim, N. T. Eldabe, M. Y. Abouzeid & M. E. Ouaf*
Department of Mathmatics, Faculty of Education, Ain Shams University, Roxy, Cairo, Egypt
*E-mail: mouaf68@gmail.com

Received 23 May 2023; accepted 24 January 2024

Non-Newtonian nanofluids are widely utilized in medical and engineering fields, such as in cooling of microchips, lubrications, cancer therapy, drug delivery etc. In the present article, we focused on the electro-osmotic effect on the peristaltic transport of a non-Newtonian nanofluid inside a horizontal micro-channel. The fluid obeys Williamson model, flowing through a porous medium with modified Darcy's law. In addition, the effects of a chemical reaction with the contribution of activation energy are taken in consideration. Furthermore, in the case of modified Darcy's law, the apparent viscosity of the fluid is used in the governing equations. Furthermore, when temperature of the hot wall tube is less than three times that of the cold wall, the term of the activation energy is simplified by using Taylor expansion.The governing equations that illustrate the velocity, temperature, and concentration of nanoparticles distributions are considered and simplified under the assumptions of a long wavelength and low Reynolds number. The homotopy perturbation method is used as semi-analytical solution for the governing equations. Moreover, some figures are used to illustrate and discuss the role of physical parameters entering the problem on the obtained solutions. Since, most of non-Newtonian fluids are viscoelastic materials, it is important to discuss the effect of Weissenberg number that represents product of strain rate and relaxation time. It is found that Weissenberg number has dual effects on the axial velocity as well as the temperature and the concentration distributions. In addition, according to Fick's law of diffusion; the temperature and concentration distributions should have opposite effects, however, it is found that the increases in the thermophoresis parameter increases both temperature and concentration distributions. This means the nanoparticles are more concentrated when migrates from one side of the tube to the other side. Furthermore, the graphs illustrate the dissimilar effect of the activation energy and the rate of the chemical reaction on the concentration of nanoparticles.

Keywords: Activation energy**,** Electro-osmotic, Modified Darcy's law, Nanofluid, Non-Newtonian fluid, Peristaltic flow

Introduction

Peristaltic flow is a muscle-controlled flow of the fluid contained in a distensible channel where periodic wave of contraction and expansion travels along the walls. In physiology, peristaltic pumping is widely occurs in the swallowing of food through the esophagus, the movement of chyme through the intestine, intra-uterine fluid motion, the transport of bile, spermatic flow in the male reproductive tract and the movement of eggs in the fallopian tube, etc. Moreover, this flow is also involved in numerous industrial applications such as rollers, hose and tube pumps and biomedical applications such as dialysis, open-heart bypass and heart-lung machines. In 1966, Latham carried out the first investigation for this type of flow; later many researchers studied the peristaltic flow of fluid under different circumstances[1].

Sharma et al.[2] examined the Magneto-hydrodynamic (MHD) flow of blood in an inclined stenosed artery. In their study the blood obeys Casson model. Ram et al.[3] studied the MHD peristaltic flow of Swine flu virus through the saliva in Oesophagus. In their study saliva is a non-Newtonian fluid that obeys Jeffrey model that carries the nano-size virus particles. Ram et al.[4] modulated a mathematical model for the peristaltic transportation of blood-borne virus through the blood stream.In their study, the blood is non-Newtonian fluid that obeys couple stressmodel and carries the nanoparticles of blood-borne virus. Abdelmoneim et al.[5] investigated the peristaltic transport of a Papanastasiou nanofluid within an inclined uniform channel in the presence of various external effects such as electroosmosis, modified Darcy's law, Dufour and Soret effects, mixed convection, chemical reactions. Eldabe et al.[6] used homotopy perturbation method (HPM) to solve the governing equations the MHD peristaltic flow Bingham nanofluid through a non-uniform inclined

duct. In addition, the impacts of thermal radiation, thermal diffusion and chemical reaction were considered.

Non-Newtonian fluid has a complex rheology (deformation) as its strain and the applied shear stress are in nonlinear relationship, such as polymer solutions, blood, greases, pastes, etc. It is intractable for a single model to exhibit all properties of non-Newtonian fluids. Hence, there are several models that are used to study the flow of non-Newtonian fluids. Over time, non-Newtonian models have been used to study the behavior of fluids, as most fluids in nature are non-Newtonian; to entrench the scientific value of the researches. Ismael et al.[7] studied the MHD peristaltic flow of a non-Newtonian micropolar nanofluid between two horizontal co-axial channels under the influence of Darcy's porous law, chemical reaction, and viscous and Ohmic dissipations. Eldabe et al.[8] studied the peristaltic flow of a non-Newtonian third-grade nanofluid inside asymmetric channel in the presence of radially varying magnetic field besides the effects of mixed convection and thermal radiation. Hayat et al.[9] studied the peristaltic flow of non-Newtonian Carreau-Yasuda nanofluid inside asymmetric duct under the influence of mixed convective, Brownian motion and thermophoresis effects. Mishra et al.[10] studied the MHD cilia flow of Jeffery nanofluid in a porous medium through an inclined channel. In addition various effects were considered such as inclined magnetic field, thermophoresis, Brownian motion, porous medium, chemical reactions, and activation energy. There are also some other interesting researches that focused on the flow of non-Newtonian fluids are reported.[11-15].

A pseudoplastic (shear thinning) materials are a non-Newtonian fluid that behave like plastic materials (can be molded) as its viscosity decreases with increasing rate of shear stress, such as ketchup, yogurt, whipped cream, molasses, nail polish, latex paint and blood. The difference between pseudoplastic flow and ideal plastic flow is the absence of yield stress. One of the pseudoplastic models is Williamson model. In 1929, Williamson[16] presented its model to exhibit the pseudoplastic flow. In the Williamson model, the apparent viscosity starts from μ_0 at the zero shear rate and gradually decreases to μ_∞ at the shear rate tends to infinity. Williamson fluid model is commonly used to study the effects of Weissenberg number (ratio between elastic forces to the viscous forces). Nadeem and Akram[17] is one of the pioneer researches that studied the peristaltic flow of Williamson fluid. Eldabe et al.[18] studied the MHD peristaltic flow of Williamson nanofluidinside an asymmetric duct, in their study; the flow is through a non-Darcy porous medium under the influence of Hall current, viscous and Ohmic dissipations. Rashid et al.[19] used HPM to solve the momentum equation that governs the MHD peristaltic transport of Williamson fluid in a curved tube. There are other interesting researches that deal with the flow of different models of non-Newtonian fluids[20-23].

Nowadays, the advance in materials technology has made it possible to produce nanometer-size particles. In 1995, the term 'nanofluid' was firstly introduced by Choi. Nanofluids represent a new class of fluids, where nanometer-sized metals such as gold (Au) or nonmetals such as Aluminum oxide (Al_2O_3) are immersed dispersed in the fluid (base fluid). Nanofluid has enhanced thermal conductivity that are widely requested in industrial and biomedical fields such as cooling of nuclear reactors, lubrications, cancer therapy, drug delivery etc. Due to this numerous applications, the study of the flow of nanofluids gained the interest of many researchers under different external effects. Moreover, since nanoparticles may interact with each other and gather together, the effect of chemical reaction is taken in consideration in the majority of the recent studies. Eldabe et al.[24] studied the MHD peristaltic flow of a power-law nanofluid through a non-uniform inclined channel, in their study the flow is through a non-Darcy porous medium under the impacts of thermal radiation, heat generation, and Ohmic dissipation. Abou-zeid[25] studied the MHD peristaltic flow of Jeffery nanofluid, in their study the flow is through a porous media between co-axial cylinders under the influence of Ohmic and viscous dissipations, and thermal radiation. Eldabe et al.[26] studied the peristaltic flow of MHD Herschel Bulkley nanofluid in a non-uniform vertical duct, in their study the flow is through a non-Darcy porous medium and the effect of chemical reaction was considered. There are other interesting researches that deal with the flow of nanofluids[27-33].

Nanofluids can be studied theoretically or experimentally in order to control heat transfer in the process. There are two ways to simulate nanofluids, namely, single, and two-phase. Nanofluids are treated as the common pure fluids in the single-phase model, and there are not any slip velocities between the

nanoparticles and fluid molecules. In the two-phase model, the researchers consider that there are slip velocities between the nanoparticles and fluid molecules. So, there would be a variable concentration of nanoparticles in a mixture. Also, the velocity between the fluid and particles may not be vanished due to many factors such as friction between the fluid and solid particles, Brownian forces, gravity, Brownian diffusion, thermophoresis properties, and dispersion. In the single-phase model, the nanoparticles can be easily fluidized, and therefore, it can be assumed that the motion slip between the phases would be considered negligible. In the present study, we assume the two-phase model, i.e., both Brownian and thermophoresis effects will appear in the governing equations system.

More than two centuries ago, Ferdinand Friedrich Reuss carried out the first investigation of moving water through a porous clay due to the presence of an external electric field. The primary important outcome was the ability of flow of water solely through application of an external electric field and without any mechanical parts. The flow according to this principle was later called electrokinetic transport. Electroosmosis is one of the electrokinetic phenomena where the bulk liquid in a micro-channel flows with respect to the walls due to the influence of an external electric field along the axis of the channel. The liquid is an electrolyte solution that carries cations (positively charged atoms) and anions (negatively charged atoms). If the channel walls are negatively charged, hence they pull cations from the electrolyte solution and repel anions, Hence the electric double layer (EDL) is formed. The ELD is composed of two distinct layers: the Stern layer, where the cations are clustered on the walls and are not allowed to move due to strong electrostatic attraction, the second layer is the Gouy-Chapman diffuse layer, where both cations and anions are clustered together but are free to move under the influence of the external electric field, dragging with them the bulk fluid which is called electroosmotic flow. The electroosmotic flow of non-Newtonian nanofluids is involved in many applications like smart sensors, food diagnostics and DNA chips[34-35]. Noreen et al[36] presented a mathematical model for the bolus electro-osmotic flow of Williamson fluid, in their study; the flow is inside an asymmetric microchannel with different zeta potentials between the walls. Prakash and Tripathi[37] studied the electroosmotic peristaltic flow of Williamson nanofluids inside a symmetric non-uniform channel under the influence of mixed convection, thermal radiation, and Dufour and Soret effects. Moatimid et al.[38] studied the electro-osmotic the peristaltic transport of biviscosity nanofluid through a micro-channel under the effects of mixed convection, thermophoresis, and Brownian diffusions. Eldabe et al.[39] focused on Newtonian nanofluid electro-osmotic peristaltic flow through horizontal symmetric channel;in their study the flow is through a porous medium in the presence of Hall currents, thermophoresis, Brownian diffusions effects and slip boundary conditions. Rafiq et al.[40] studied the electroosmotic peristaltic transport of Jeffrey nanofluid through an asymmetric channel under the impact of chemical reaction and slip conditions.

The fluid flow problems with heat and mass transfer under the effect of chemical reactions have numerous applications in metallurgy, petroleum and chemical engineering industries, such as food processing, polymer production, cooling of nuclear reactors, and the flow in a desert cooler. In 1889, Arrhenius introduced the activation energy. It is the minimum amount of energy that is required to start a chemical reaction. It may be in the form of potential energy or kinetic energy. Accordingly, in the absence of activation energy, reactants do not interact and cannot form products. Activation energy is widely involved in chemical engineering, geothermal and mechanics of water and oil emulsions. Ellahi et al.[41] studied the peristaltic flow of couple stress nanofluid in a coaxial tube, under the influence of chemical reaction with activation energy effects. Ibrahim et al.[42] focused on the MHD peristaltic pumping of Bingham nanofluid through a non-Darcy porous medium, in the presence of chemical reaction with activation energy effects.

In the present study, the pseudoplastic nanofluid obeys Williamson model, the flow is inside a horizontal channel with peristalsis movement along the walls of the channel. Moreover, due to the presence of external electric field, electro-osmotic is considered. In addition to, the flow is through a porous medium that obeys modified Darcy's law, where the apparent viscosity of the fluid is used in the porous term instead of the Newtonian viscosity. Also interaction between the nanoparticles is not neglected, therefore the effects of chemical reaction with activation energy are considered. To our best of knowledge, this model is not studied so far.

Furthermore, in the absence of the modified Darcy porous medium our model bears resemblance to the issue investigated by Eldabe et al.[18].

Mathematical formulation of the problem

The two-dimensional peristaltic flow of Williamson nanofluid, the flow is through a porous medium inside a horizontal duct, in the presence of external electric filed is investigated. The porous medium obeys modified Darcy's law, and the effects of Electro-osmotic phenomenon, chemical reaction and activation energy are taken into consideration. Cartesian coordinates (X,Y) in the fixed laboratory frame are chosen, where X-axis denotes the axis of the tube. Fig. 1 represents the problem where the dot lines represent the elastic walls of the channel and the solid lines represent the sinusoidal waves (peristaltic transport) along the walls. The lower wall has temperature T_0 and the solute concentration is C_0 while the upper wall has temperature T_1 and the solute concentration is C_1. The geometrical shape of the wall deformation is defined by:

$$H(X,t)=h+a\sin\left(\frac{2\pi}{\lambda}(X-\bar{c}t)\right), \quad \text{... (1)}$$

The vector forms of the governing equations[5] are:

$$\nabla.\vec{V}=0, \quad \text{... (2)}$$

$$\rho_f\left(\frac{\partial}{\partial t}+\vec{V}\nabla\right)\vec{V}=-\nabla P+\nabla.\vec{\tau}+\vec{R}+\rho_e\vec{E}, \quad \text{... (3)}$$

$$(\rho c)_f\left(\frac{\partial}{\partial t}+\vec{V}\nabla\right)T=K\nabla^2T+\vec{\tau}.\nabla\vec{V}+(\rho c)_p\left\{D_B(\nabla T\nabla C)+\frac{D_T}{T_0}(\nabla^2T)\right\}+\xi\vec{E}^2 \quad \text{... (4)}$$

$$\left(\frac{\partial}{\partial t}+\vec{V}\nabla\right)C=D_B(\nabla^2C)+\frac{D_T}{T_0}(\nabla^2T)-A\left(\frac{T}{T_1}\right)^n Exp\left[\frac{-E_a}{K_BT}\right](C-C_1), \quad \text{... (5)}$$

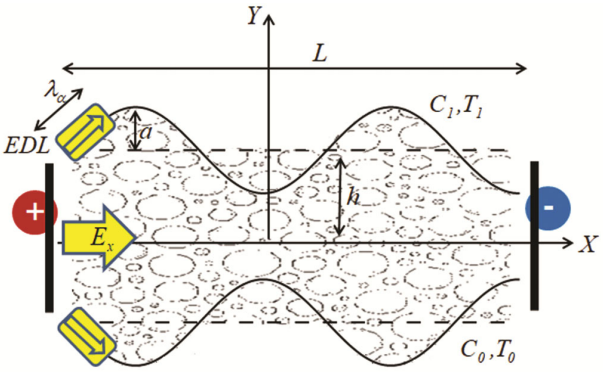

Fig. 1 — Physical model and coordinates system

where,

$$\vec{V}=(U(X,Y,t),\ V(X,Y,t)), \quad \text{... (6)}$$

$$\vec{E}=(E_x,0), \quad \text{... (7)}$$

$$\vec{R}=-\frac{\mu(\gamma)}{k}\vec{V}. \quad \text{... (8)}$$

For incompressible non-Newtonian fluid with the relation between $\vec{\tau}$ and $\vec{\gamma}$ is:

$$\vec{\tau}=\mu\vec{\gamma}, \quad \text{... (9)}$$

where,

$$\vec{\gamma}=\nabla\vec{V}+(\nabla\vec{V})^T, \quad \text{... (10)}$$

$$\nabla\vec{V}=\begin{pmatrix}\partial U/\partial X & \partial U/\partial Y\\ \partial V/\partial X & \partial V/\partial Y\end{pmatrix},$$

$$(\nabla\vec{V})^T=\begin{pmatrix}\partial U/\partial X & \partial V/\partial X\\ \partial U/\partial Y & \partial V/\partial Y\end{pmatrix}, \quad \text{... (11)}$$

$$\gamma=\sqrt{\frac{1}{2}tr(\vec{\gamma}^2)}, \quad \text{... (12)}$$

From literature[18] the apparent viscosity of Williamson fluid is written as:

$$\mu\equiv\mu(\gamma)=\mu_\infty+\frac{\mu_0-\mu_\infty}{1-\Gamma\gamma}=\mu_\infty+(\mu_0-\mu_\infty)(1-\Gamma\gamma)^{-1}, \quad \text{... (13)}$$

Taking the case for which $\mu_\infty=0$ and $\Gamma\gamma<1$, applying Taylor expansion, then it becomes

$$\mu\equiv\mu_0(1+\Gamma\gamma)=\mu_0\left(1+\Gamma\sqrt{\left(\frac{\partial U}{\partial Y}+\frac{\partial V}{\partial X}\right)^2+2\left(\left(\frac{\partial U}{\partial X}\right)^2+\left(\frac{\partial V}{\partial Y}\right)^2\right)}\right) \quad \text{... (14)}$$

Also from Eqs. 9 and 10 $\nabla.\vec{\tau}$ is written as :

$\nabla.\vec{\tau}=\nabla.(\mu\vec{V})+\nabla.(\mu\vec{V}^T)$ and it becomes:

$$\nabla.\vec{\tau}=\left\{\mu\left(\frac{\partial^2U}{\partial X^2}+\frac{\partial^2U}{\partial Y^2}\right)+2\frac{\partial\mu}{\partial X}\frac{\partial U}{\partial X}+\frac{\partial\mu}{\partial Y}\left(\frac{\partial U}{\partial Y}+\frac{\partial V}{\partial X}\right)\right\}$$

$$i+\left\{\mu\left(\frac{\partial^2V}{\partial X^2}+\frac{\partial^2V}{\partial Y^2}\right)+2\frac{\partial\mu}{\partial Y}\frac{\partial V}{\partial Y}+\frac{\partial\mu}{\partial X}\left(\frac{\partial U}{\partial Y}+\frac{\partial V}{\partial X}\right)\right\}j \quad \text{... (15)}$$

Maxwell's equations are a set of fundamental equations that describe how electric and magnetic fields interact and propagate in space. One of these equations is:

$$\nabla\cdot\vec{E}=\frac{\rho_e}{\varepsilon}. \quad \text{... (16)}$$

In the context of electrochemistry and electrostatics, it is possible to regard the electric field as a conservative field. This implies that it can be represented as the gradient of a scalar potential function, which is commonly referred to as the electric potential:

$$\vec{E} = -\nabla\phi \qquad \text{... (17)}$$

Using Eq.16 into Eq. 17, hence

$$\nabla^2\phi = -\frac{\rho_e}{\varepsilon}\ , \qquad \text{... (18)}$$

Considering a symmetric binary electrolyte solution,

$$\rho_e = e\,z\left(n^+ - n^-\right), \qquad \text{... (19)}$$

Considering no EDL overlap, hence, the number of densities of cations and anions are given by Boltzmann distribution:

$$n^{\pm} = N_0\ Exp\left[\mp\frac{e\,z\phi}{k_B T_{av}}\right]. \qquad \text{... (20)}$$

Using Eq. 20 into Eq. 19, therefore Eq.18 can be written as:

$$\nabla^2\phi = \frac{2\,N_0 e\,z}{\varepsilon}\,Sinh\left[\frac{e\,z}{k_B T_{av}}\phi\right]. \qquad \text{... (21)}$$

The exact solutions of the Poisson–Boltzmann (P–B) equation described above often require the use of special functions or specific assumptions, which can make them impractical for practical applications. To address this limitation, researchers have developed several approximate solutions for the P–B equation. One of the well-known approximations is derived from the widely recognized Debye–Hückel (DH) linear approximation. Essentially, the DH approximation employs a linear connection between ion concentration and electric potential, serving as a substitution for the original non-linear Boltzmann-type correlation between these variables. However, this approximation is suitable for situations characterized by low zeta potential conditions. This approach is commonly employed in scientific literature due to its straightforward and efficient computational process[43].

Consequently, considering the value of ϕ is small enough to apply the Debye-Huckel linearization approximation, the equation can be simplified as follows:

$$\nabla^2\phi = \frac{2\,N_0 e^2 z^2}{\varepsilon\,k_B T_{av}}\phi\,. \qquad \text{... (22)}$$

The fixed frame (X,Y) can be transformed to the moving frame (x,y) by using the following transformations

$$\left.\begin{aligned} x &= X - \bar{c}t,\\ Y &= y,\\ u &= U - \bar{c},\\ v &= V\\ p(x) &= P(X,t) \end{aligned}\right\} \qquad \text{... (23a)}$$

The governing equations in the moving frame are:

$$\frac{\partial u}{\partial x} + \frac{\partial v}{\partial y} = 0\,, \qquad \text{... (23b)}$$

$$\rho_f\left(u\frac{\partial u}{\partial x} + v\frac{\partial u}{\partial y}\right) = \frac{-\partial P}{\partial x} + \mu\left(\frac{\partial^2 u}{\partial x^2} + \frac{\partial^2 u}{\partial y^2}\right) + 2\frac{\partial\mu}{\partial x}\frac{\partial u}{\partial x} + \frac{\partial\mu}{\partial y}\left(\frac{\partial u}{\partial y} + \frac{\partial v}{\partial x}\right) - \varepsilon\left(\frac{\partial^2\phi}{\partial x^2} + \frac{\partial^2\phi}{\partial y^2}\right)E_x + R_x\ , \qquad \text{... (24)}$$

$$\rho_f\left(u\frac{\partial v}{\partial x} + v\frac{\partial v}{\partial y}\right) = \frac{-\partial P}{\partial y} + \mu\left(\frac{\partial^2 v}{\partial x^2} + \frac{\partial^2 v}{\partial y^2}\right) + 2\frac{\partial\mu}{\partial y}\frac{\partial v}{\partial y} + \frac{\partial\mu}{\partial x}\left(\frac{\partial u}{\partial y} + \frac{\partial v}{\partial x}\right) + R_y\,, \qquad \text{... (25)}$$

$$(\rho c)_f\left(u\frac{\partial T}{\partial x} + v\frac{\partial T}{\partial y}\right) = k_c\left(\frac{\partial^2 T}{\partial x^2} + \frac{\partial^2 T}{\partial y^2}\right) + \mu\left\{\left(\frac{\partial u}{\partial y} + \frac{\partial v}{\partial x}\right)^2 + 2\left[\left(\frac{\partial u}{\partial x}\right)^2 + \left(\frac{\partial v}{\partial y}\right)^2\right]\right\}, + (\rho c)_p\left\{D_B\left(\frac{\partial T}{\partial x}\frac{\partial f}{\partial x} + \frac{\partial T}{\partial y}\frac{\partial f}{\partial y}\right) + \frac{D_T}{T_{av}}\left[\left(\frac{\partial T}{\partial x}\right)^2 + \left(\frac{\partial T}{\partial y}\right)^2\right]\right\} + \xi\,E_x^2 \qquad \text{... (26)}$$

$$u\frac{\partial C}{\partial x} + v\frac{\partial C}{\partial y} = D_B\left(\frac{\partial^2 C}{\partial x^2} + \frac{\partial^2 C}{\partial y^2}\right) + \frac{D_T}{T_m}\left(\frac{\partial^2 T}{\partial x^2} + \frac{\partial^2 T}{\partial y^2}\right) - A\left(\frac{T}{T_1}\right)^n Exp\left[\frac{-E_a}{K_B T}\right](C - C_1) \qquad \text{... (27)}$$

From Eq. 8 the term R_x and R_y are defined as:

$$\left.\begin{aligned} R_x &= -\frac{\mu}{k}(u+\bar{c}) = -\frac{\mu_0}{k}\left(1 + \Gamma\sqrt{\left(\frac{\partial U}{\partial Y} + \frac{\partial V}{\partial X}\right)^2 + 2\left(\left(\frac{\partial U}{\partial X}\right)^2 + \left(\frac{\partial V}{\partial Y}\right)^2\right)}\right)\\ R_y &= -\frac{\mu}{k}v = -\frac{\mu_0}{k}\left(1 + \Gamma\sqrt{\left(\frac{\partial U}{\partial Y} + \frac{\partial V}{\partial X}\right)^2 + 2\left(\left(\frac{\partial U}{\partial X}\right)^2 + \left(\frac{\partial V}{\partial Y}\right)^2\right)}\right)v \end{aligned}\right\} \qquad \text{... (28)}$$

It is clear that in the case of Newtonian fluid (where $\Gamma = 0$), the modified Darcy's term will be reduced to the ordinary Darcy porous term

$$\vec{R} = -\frac{\mu_0}{k}\vec{V}\ . \qquad \text{... (29)}$$

The appropriate boundary conditions correlated to the governing equations in the moving frame are:

$$\left.\begin{array}{l} T = T_0,\ C = C_0,\ u = -\bar{c},\quad at\ y = -H = -\left(h + aSin\left(\frac{2\pi}{\lambda}x\right)\right) \\ T = T_1,\ C = C_1,\quad u = -\bar{c},\quad at\ y = H = h + aSin\left(\frac{2\pi}{\lambda}x\right) \end{array}\right\}, \quad \text{... (30)}$$

The boundary conditions associated to the wall zeta potential ϕ are:

$$\varphi = \zeta \quad at\ y = H\ ,\quad \frac{\partial \varphi}{\partial y} = 0 \quad at\ y = 0 \quad \text{... (31)}$$

Eq. (31) implies that the fluid particles closest to the solid boundary of channel are travelling equal displacements in equal times in the opposite direction. While, Eq. (32) means that there is a constant zeta potential on the solid boundary and a maximum value is exist on the symmetric axis of channel. Considering Considering

$$u = \frac{\partial \psi}{\partial y} \text{ and } v = -\frac{\partial \psi}{\partial x} \quad \text{... (32)}$$

Now, we shall introduce the following dimensionless quantities:

$$\left.\begin{array}{l} x^* = \frac{x}{\lambda},\ y^* = \frac{y}{h},\ \psi^* = \frac{\psi}{\bar{c}h},\ \omega = \frac{a}{h},\ \delta = \frac{h}{\lambda},\ P^* = \frac{h^2 P}{\lambda \bar{c} \mu_0},\ \theta\ \frac{T - T_1}{T_0 - T_1},\ H^* = \frac{H}{h},\ k^* = \frac{k}{h^2}, \\ f = \frac{C - C_1}{C_0 - C_1},\ W_e = \frac{\Gamma \bar{c}}{h},\ Re = \frac{\rho_f \bar{c}\, h}{\mu_0},\ Pr = \frac{\mu_0 c_f}{k_c},\ Ec = \frac{\bar{c}^2}{c_f (T_0 - T_1)},\ \varphi = \frac{\varphi^*}{\zeta},\ \beta = \frac{T_0}{T_1}, \\ k_\alpha = \frac{A h^2}{\nu_\mu},\ Sc = \frac{\nu_\mu}{D_B},\ E_A = \frac{E_a}{K_B T_1},\ N_b = \frac{D_B (C_0 - C_1)(\rho c)_p}{\mu_0 c_f},\ N_t = \frac{D_T (T_0 - T_1)(\rho c)_p}{T_{av} \mu_0 c_f}, \\ S = \frac{\xi h^2 E_x{}^2}{k_c (T_0 - T_1)},\ U_{HS} = -\frac{E_x \varepsilon \zeta}{\mu_0 \bar{c}},\ \Omega = h\, z\, e \sqrt{\frac{2 N_0}{\varepsilon k_B T_{av}}} \end{array}\right\} \quad \text{... (33)}$$

Considering low Reynolds number and long wave length (Re or δ are neglected).

Thereby, after dropping the star mark, the apparent viscosity becomes:

$$\mu = \mu_0 \left(1 + W_e \frac{\partial u}{\partial y}\right), \quad \text{... (34)}$$

and the dimensionless governing equations become:

$$\frac{\partial P}{\partial x} = \frac{\partial^3 \psi}{\partial y^3} + 2W_e \left(\frac{\partial^2 \psi}{\partial y^2}\right)\left(\frac{\partial^3 \psi}{\partial y^3}\right) - \frac{1}{k}\left(1 + \frac{\partial \psi}{\partial y}\right)\left(1 + W_e \frac{\partial^2 \psi}{\partial y^2}\right) + U_{HS} \frac{\partial^2 \phi}{\partial y^2}, \quad \text{... (35)}$$

$$\frac{\partial P}{\partial y} = 0, \quad \text{... (36)}$$

$$\frac{\partial^2 \theta}{\partial y^2} + Pr\, Ec \left(1 + W_e \frac{\partial^2 \psi}{\partial y^2}\right)\left(\frac{\partial^2 \psi}{\partial y^2}\right)^2 + pr\left(N_b \left(\frac{\partial \theta}{\partial y}\right)\left(\frac{\partial f}{\partial y}\right) + N_t \left(\frac{\partial \theta}{\partial y}\right)^2\right) + S = 0, \quad \text{... (37)}$$

$$\frac{\partial^2 f}{\partial y^2} + \frac{N_t}{N_b}\frac{\partial^2 \theta}{\partial y^2} - Sc\, k_\alpha (1 + (\beta - 1)\theta)^n\ Exp\left[\frac{-E_A}{1 + (\beta - 1)\theta}\right] f = 0 \quad \text{... (38)}$$

The non-dimensional boundary conditions correlated to the governing equations are:

$$\left.\begin{array}{ll} \theta = 1,\ f = 1,\ \frac{\partial \psi}{\partial y} = -1, & at\ y = -H = -1 - \omega\ Sin(2\pi\pi) \\ \theta = 0,\ f = ,0\ \frac{\partial \psi}{\partial y} = -1, & at\ y = H = 1 + \omega\ Sin(2\pi\pi) \\ \psi = 0\ , & at\ y = 0 \end{array}\right\}, \quad \text{... (39)}$$

and the dimensionless boundary conditions associated to ϕ are :

$$\varphi = 1 \quad at\ y = H = 1 + \omega\ Sin(2\pi\pi)\ ,\quad \frac{d\varphi}{dy} = 0 \quad at\ y = 0 \quad \text{... (40)}$$

Since, the dimensionless equation of Eq. 21is :

$$\frac{\partial^2 \phi}{\partial y^2} = \Omega^2\, \phi\,. \quad \text{... (41)}$$

And after using the dimensionless boundary conditions in Eq. 40, then the solution of Eq. 41 can be written in the non-dimensional form as:

$$\phi = \frac{Cosh(\Omega\, y)}{Cosh(\Omega\, H)} \quad \text{... (42)}$$

Hence, the Eq.36 becomes:

$$\frac{\partial P}{\partial x} = \frac{\partial^3 \psi}{\partial y^3} + 2W_e \left(\frac{\partial^2 \psi}{\partial y^2}\right)\left(\frac{\partial^3 \psi}{\partial y^3}\right) - \frac{1}{k}\left(1 + \frac{\partial \psi}{\partial y}\right)\left(1 + W_e \frac{\partial^2 \psi}{\partial y^2}\right) + \frac{\Omega^2\, U_{HS}}{Cosh(\Omega\, H)} Cosh(\Omega\, y), \quad \text{... (43)}$$

Considering $(\beta - 1) << 1$ and using Taylor expansion, Hence Eq. 38 becomes

$$\frac{\partial^2 f}{\partial y^2} + \frac{N_t}{N_b}\frac{\partial^2 \theta}{\partial y^2} - Sc\, k_\alpha e^{-E_A}(1 + n(\beta - 1)\theta)(1 + E_A(\beta - 1)\theta) f = 0 \quad \text{... (44)}$$

Again using $(\beta - 1) << 1$, then Eq. 44 becomes:

$$\frac{\partial^2 f}{\partial y^2} + \frac{N_t}{N_b}\left(\frac{\partial^2 \theta}{\partial y^2}\right) = Sc k_\alpha e^{-E_A}(1 + (n + E_A)(\beta - 1)\theta) f \quad \text{... (45)}$$

Method of solution

The governing Eqs. (43), (37) and (45) form a system of non-linear partial differential equations with boundary conditions (36), to solve this system, homotopy perturbation method (HPM) was used. Since $\psi \equiv \psi(x, y)$, $\theta \equiv \theta(x, y), f \equiv f(x, y)$ where $y \equiv H(x)$, therefore by considering a vertical slice of the channel by taking $\omega\, Sin(2\,\pi\, x) = 0.2$, the boundary conditions are fixed at $y = \pm H = 1.2$, Consequently, the system of governing equations is considered as a system ordinary differential equations (O.D.E).

Considering ω_p is a small parameter, such that $0 < \omega_p \leq 1$ so that:

$$\frac{d^3\psi}{dy^3} - \frac{\partial^3\psi_{00}}{\partial y^3} + \omega_p \frac{\partial^3\psi_{00}}{\partial y^3} = \omega_p \begin{Bmatrix} \left(\frac{dP}{dx} - 2W_e\left(\frac{d^2\psi}{dy^2}\right)\left(\frac{d^3\psi}{dy^3}\right) + \frac{1}{k}\left(1 + \frac{d\psi}{dy}\right)\left(1 + W_e\frac{d^2\psi}{dy^2}\right)\right), \\ -\frac{\Omega^2 U_{HS}}{Cosh(\Omega H)} Cosh(\Omega y) \end{Bmatrix}, \quad \text{... (46)}$$

$$\frac{d^2\theta}{dy^2} - \frac{\partial^2\theta_{00}}{\partial y^2} + \omega_p \frac{\partial^2\theta_{00}}{\partial y^2} + \omega_p \left\{ Pr\,Ec\left(1 + W_e\frac{d^2\psi}{dy^2}\right)\left(\frac{d^2\psi}{dy^2}\right)^2 + pr\left(N_b\left(\frac{d\theta}{dy}\right)\left(\frac{df}{\partial y}\right) + N_t\left(\frac{d\theta}{dy}\right)^2\right) + S \right\} = 0, \quad \text{... (47)}$$

$$\frac{d^2 f}{dy^2} - \frac{\partial^2 f_{00}}{\partial y^2} + \omega_p \frac{\partial^2 f_{00}}{\partial y^2} + \omega_p \left\{ \frac{N_t}{N_b}\frac{d^2\theta}{dy^2} - Sc\,k_\alpha e^{-E_A}\left(1 + n(\beta-1)\theta\right)\left(1 + E_A(\beta-1)\theta\right) f \right\} = 0 \quad \text{... (48)}$$

where,

$$\left.\begin{aligned} \psi(y) &= \psi_0 + \omega_p\,\psi_1 + \omega_p{}^2\psi_2 + \ldots \\ \theta(y) &= \theta_0 + \omega_p\,\theta_1 + \omega_p{}^2\theta_2 + \ldots \\ f(y) &= f_0 + \omega_p\,f_1 + \omega_p{}^2 f_2 + \ldots \end{aligned}\right\}. \quad \text{... (49)}$$

Considering the boundary conditions (39), we got the initial approximations (zero order) of the equations (46- 49) as follows:

$$\psi_{00} = \frac{1}{6}\left(\frac{\partial P}{\partial x} + \frac{1}{k}\right)y^3 - \left(1 + \frac{h^2}{2}\left(\frac{\partial P}{\partial x} + \frac{1}{k}\right)\right)y,$$

$$\theta_{00} = \frac{S}{2}y^2 - \frac{1}{2h}y + \frac{1}{2}\left(1 - Sh^2\right) \text{ and } f_{00} = -\frac{1}{2h}y + \frac{1}{2}$$

The zero, first and second orders solutions for the stream function ψ, temperature distribution θ and nanoparticles concentration ϕ are computed. Hence at $\omega_p = 1$ we got the solution form for the functions (49) as follows:

$$u(y) = A_0 y^8 + A_1 y^7 + A_2 y^6 + A_3 y^5 + A_4 y^3 + A_5 y^2 + A_6 y + A_7 + A_8 Cosh[\Omega y] + A_9 y Cosh[\Omega y] + A_{10} Sinh[\Omega y] + A_{11} y^2 Sinh[\Omega y], \quad \text{... (50)}$$

$$\theta(y) = A_{12} y^8 + A_{13} y^7 + A_{14} y^6 + A_{15} y^5 + A_{16} y^4 + A_{17} y^3 + A_{18} y^2 + A_{19} y + A_{20} + A_{21} Sinh[\Omega y] + A_{22} y Sinh[\Omega y] + A_{23} y^2 Sinh[\Omega y], \quad \text{... (51)}$$

$$f(y) = A_{24} y^8 + A_{25} y^8 + A_{26} y^7 + A_{27} y^6 + A_{28} y^5 + A_{29} y^4 + A_{30} y^3 + A_{31} y^2 + A_{32} y + A_{33} \quad \text{... (52)}$$

The constants $A_0 \to A_{33}$ are functions in the entering physical parameters and they are available upon request from the authors.

Results and Discussion

We studied the flow of the peristaltic flow of the Williamson nanofluid in the presence of various external effects. The most novel terms in our model is modified Darcy porous medium, electroosmosis and the simplified activation energy.In the momentum governing equation (Eq. 43) the terms $\left(1 + W_e\frac{\partial^2\psi}{\partial y^2}\right)$ and $\frac{\Omega^2 U_{HS}}{Cosh(\Omega H)} Cosh(\Omega y)$ are related to the presence of the modified Darcy porous medium and the electroosmotic flow respectively. In addition the right hand side of the concentration governing equation (Eq. 45) is related to the presence of the presence of the activation energy.

The system of governing equations for velocity, temperature and concentration was solved by HPM method, and to support the results, the effects of various parameters entering the problem are discussed through the Figs. (2)–(14). Physically; nanoparticles are good conductors of heat, therefore Prandtl number Pr is fixed at a small value to catch up with the strong thermal diffusivity. In addition Weissenberg number is fixed at a small value to satisfy the domination of viscous forces. Moreover, Electroosmotic parameter Ω is fixed at a large value to emphasize thin electric double layer (EDL)[8, 18, 44]. The graphs show that u is always negative and its curve has a minimum peak. This means that the flow is in the negative direction of x-axis (retarded flow). Hence, the axial velocity u decreases (increases in its negativity) along the path form the lower wall $(y = -H)$ to the upper wall $(y = H)$.

Fig. 2 shows that the velocity is highly affected by the permeability parameter, it is found that u decreases in its negativity as k increases, this behavior is in agreement with Eldabe et al.[1]. Physically, in the absence of permeability $(k \to \infty)$,it is found that the axial velocity of this model aligns with the positive direction of x-axis. Hence, as k increases the flow in the negative direction is damped and the curve of u goes flatten.

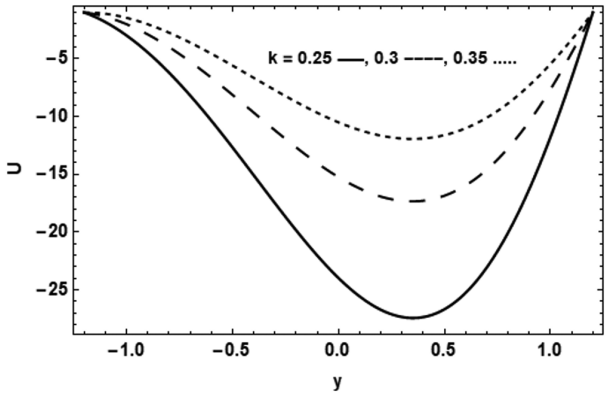

Fig. 2 — The velocity distribution u for different values of k where $h=1.2$, $\partial p/\partial x=1$, $W_e=0.1$, $U_{HS}=3$, $\Omega=2$, $S=1.5$, $\omega=1.03$, $N_t=0.4$, $N_b=0.3$, $Ec=2$, $Pr=0.5$, $Sc=0.5$, $E_A=0.5$, $k_\alpha=0.8$, $n=2$

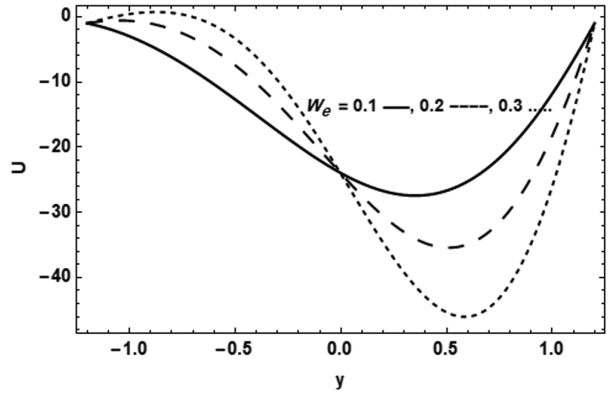

Fig. 3 — The velocity distribution u for different values of W_e where $h=1.2$, $\partial p/\partial x=1$, $W_e=0.1$, $\Omega=2$, $S=1.5$, $\omega=1.03$, $N_t=0.4$, $N_b=0.3$, $Ec=2$, $Pr=0.5$, $Sc=0.5$, $E_A=0.5$, $k_\alpha=0.8$, $n=2$, $k=0.3$

Fig. 3 shows that in the lower region (below the axis of the tube) u decreases as W_e increases while the effect is revised in the other side. The dual effect behavior is in agreement with Noreen et al[36] and Akbar[45]. Physically, pseudoplastic fluids are viscoelastic materials in which the yield stress is absent, Weissenberg number represents the ratio between elastic forces to the viscous forces, and it is simplified to be defined as the strain rate multiplied by the relaxation time, where the relaxation time is the time taken by the fluid to inherit the flow under the applied share stress[46]. Near the lower wall; the fluid layers gain energy from the hot wall, here as W_e increases the relaxation time increases and the strain rate decreases, hence the axial velocity decreases (less negativity). In contrast, near the upper wall; the fluid layers lose its energy, here as W_e increases the relaxation time decrease and the strain rate increases, hence the axial velocity increases (more negativity).

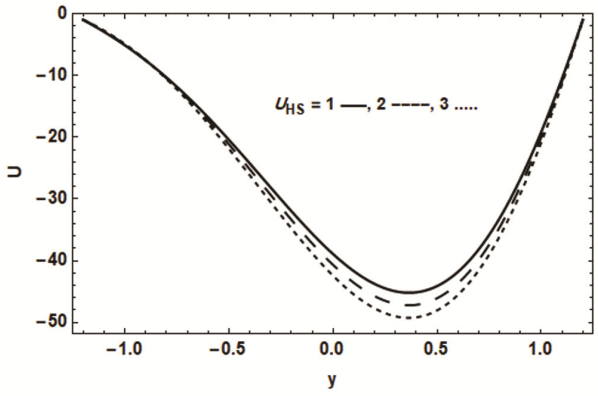

Fig. 4 — The velocity distribution u for different values of U_{HS} where $h=1.2$, $\partial p/\partial x=1$, $W_e=0.1$, $k=0.3$, $\Omega=2$, $S=1.5$, $\omega=1.03$, $N_t=0.4$, $N_b=0.3$, $Ec=2$, $Pr=0.5$, $Sc=0.5$, $E_A=0.5$, $k_\alpha=0.8$, $n=2$

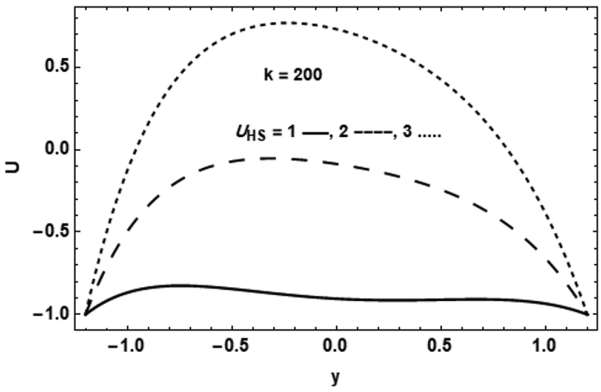

Fig. 5 — The velocity distribution u for different values of U_{HS} where $k=200$ $h=1.2$, $\partial p/\partial x=1$, $W_e=0.1$, $k=0.3$, $\Omega=2$, $S=1.5$, $\omega=1.03$, $N_t=0.4$, $N_b=0.3$, $Ec=2$, $Pr=0.5$, $Sc=0.5$, $E_A=0.5$, , $n=2$

Fig. 4 shows that u increases in its negativity as U_{HS} increases. On the other hand, in the absence of permeability $(k\to\infty)$, the direction of the axial velocity is reversed and Fig. 5 shows that u increases in the positive direction as U_{HS} increases. This agrees with Chaube et al.[47] and Ahmed et al.[48]. Physically, when the wall comes into contact with the electrolyte solution, it becomes electrically charged. This charged surface has a tendency to attract cations (ions

with a positive charge) and repel anions (ions with a negative charge). When an electric field is applied, the mobile cations located near the wall, within the diffuse layer of the electric double layer (EDL), start moving towards the cathode. This movement simultaneously induces the bulk fluid to flow in the same direction, resulting in what is known as Electrophoretic or Electroosmotic Flow (EOF). As a result, the EOF occurs in the positive direction of the X-axis. As a result, (as seen in Fig. 5) when U_{HS} increases the EOF increase which supports the net flow. While Fig. 4 reveals that in the presence of permeability the direction of the axial fluid as well as the direction of the EOF is reversed and hence when U_{HS} increases the EOF increase which supports the net flow in the negative direction.

The graphs of temperature distribution θ satisfy the boundary conditions and illustrate that the curve of θ has a minimum point. Physically, although $(T_0 > T_1)$ is confirmed, there are still two other possible scenarios to consider. In one case, it could be $(T > T_1)$, and in the other case, it could be $(T < T_1)$. If it turns out to the 2nd case, then $\left(\theta = \frac{T - T_1}{T_0 - T_1} < 0\right)$ which implies that the cooling process will initiate first, followed by the heating process.Therefore, the curve of θ exhibits a minimum point (negative temperature distribution).

Fig. 6 depicts that θ increases in the negative direction (decreases) as Ec increases, this behaviour is in agreement with Eldabe et al.[25,26], Eldabe and Abouzeid [49], and Mohamed and Abozeid[50, 51].

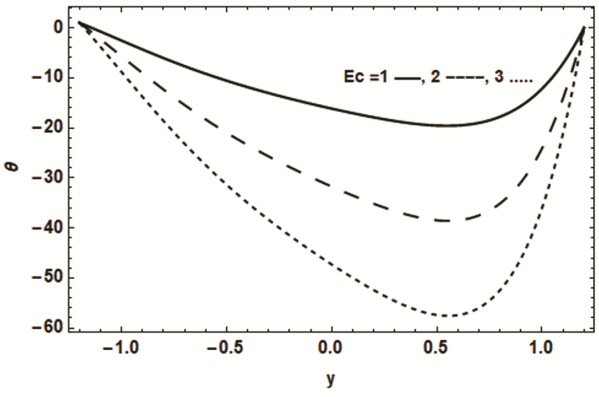

Fig. 6 — The temperature distribution θ for different values of Ec where $h = 1.2$, $\partial p/\partial x = 1$, $W_e = 0.1$, $U_{HS} = 3$, $\Omega = 2$, $S = 1.5$, $\omega = 1.03$, $N_t = 0.4$, $N_b = 0.3$, $k = 0.3$, $Pr = 0.5$, $Sc = 0.5$, $E_A = 0.5$, $k_\alpha = 0.8$, $n = 2$

Physically, as Ec increases the temperature near the outer peristaltic tube, accordingly the drag between the fluid particles increases. In viscous fluid, this kinetic energy generates an internal heat energy (viscous dissipation) which in terms increases the fluid temperature.

Fig. 7 show that θ increases in the negative direction (decreases) as N_t increases, this behavior is in agreement with Mohamed and Abozeid[50, 51], Abouzeid et al.[52] and Subbarayudu et al.[53]. Physically, as N_t increases the thermophoresis force is enhanced, accordingly the flow of nanoparticles from lower wall to upper wall is much better,and this additional kinetic energy increases the temperature.

Fig. 8 shows that θ decreases in the negative direction (increases) as Ω increases, this behaviour is

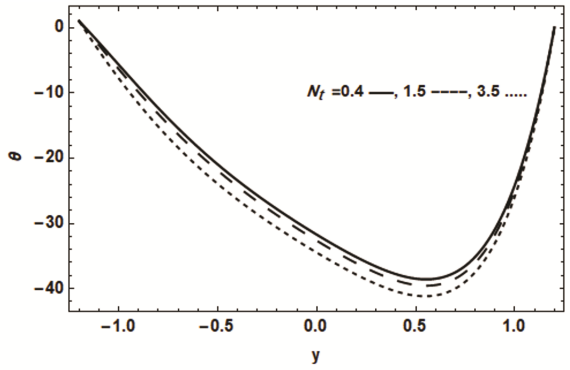

Fig. 7 — The temperature distribution θ for different values of N_t where $h = 1.2$, $\partial p/\partial x = 1$, $W_e = 0.1$, $U_{HS} = 3$, $\Omega = 2$, $S = 1.5$, $\omega = 1.03$, $k = 0.3$, $N_b = 0.3$, $Ec = 2$, $Pr = 0.5$, $Sc = 0.5$, $E_A = 0.5$, $k_\alpha = 0.8$, $n = 2$

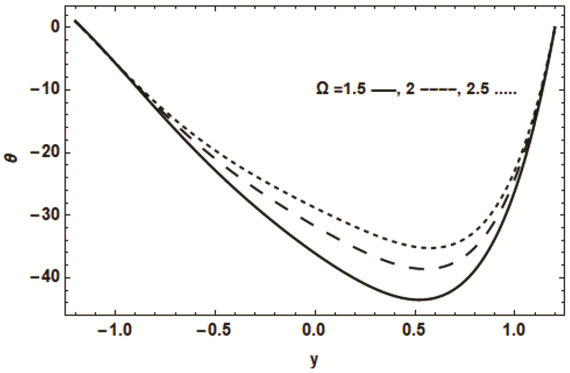

Fig. 8 — The temperature distribution θ for different values Ω of where $h = 1.2$, $\partial p/\partial x = 1$, $W_e = 0.1$, $U_{HS} = 3$, $k = 0.3$, $S = 1.5$, $\omega = 1.03$, $N_t = 0.4$, $N_b = 0.3$, $Ec = 2$, $Pr = 0.5$, $Sc = 0.5$, $E_A = 0.5$, $k_\alpha = 0.8$, $n = 2$

in agreement with Noreen et al [36]. Physically electro-osmotic parameter Ω is inversely proportional to the thickness of the EDL (Debye length), so as Ω increases the thickness of the EDL decreases, hence the net flow of the charged particles decreases, which in turns reduces the temperature.

Fig. 9 depicts that the increment in W_e has a dual effect on the temperature profile, it is found that θ increases in its negativity as We increases till a definite point then the effect is reversed. This effect is in agreement with Eldabe et al.[18]. Physically, as discussed in Fig. 3, near the lower wall; the fluid consumes much more energy too vercome its Plasticity and start the flow, hence θ decreases in its negativity. While near the upper wall; the relaxation time decreases and the flow is much better, hence the kinetic energy increases and hence θ increases in its negativity The graphs of that nanoparticles concentration f satisfy the boundary conditions and depict that the curves of f have opposite behavior to curves of θ . Physically, this behavior complies with the fact that the nanoparticles concentration increases as the temperature decreases and vice versa.

Fig. 10 shows that as N_b increases f decreases. This behaviour is in agreement with Eldabe et al.[3], Mohamed and Abozeid[50, 51], and Abou-zeid et al.[45]. Physically, the increment in N_b indicates that the random motion increases, therefore the concentration decreases.

Fig. 11 shows that as Sc increases f increases. This behaviour agrees with the observation of Sheikholeslami and Ganji[55], and Hayat et al.[56]. Physically, Schmidt number represents the ratio of momentum diffusivity (kinematic viscosity) and mass diffusivity. Hence, the concentration increases.

Fig. 12 shows that as N_t increases f increases. This behaviour is in agreement with Eldabe et al.[26] and Abozeid et al. [45]. Physically, the temperature gradient (∇T) does not just initiate heat transfer but also propels the movement of nanoparticles within the fluid. Furthermore, an increase in the thermophoresis N_t parameter signifies a strengthening of the thermophoresis force, leading to accelerated nanoparticle migration in a direction counter to the

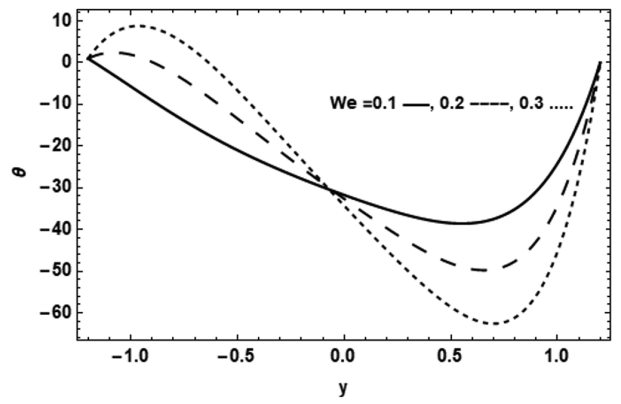

Fig. 9 — The concentration θ for different values of W_e where $h=1.2$, $\partial p/\partial x=1$, $k=0.3$, $U_{HS}=3$, $\Omega=2$, $S=1.5$, $\omega=1.03$, $N_t=0.4$, $N_b=0.3$, $Ec=2$, $Pr=0.5$, $Sc=0.5$, $E_A=0.5$, $k_\alpha=0.8$, $n=2$

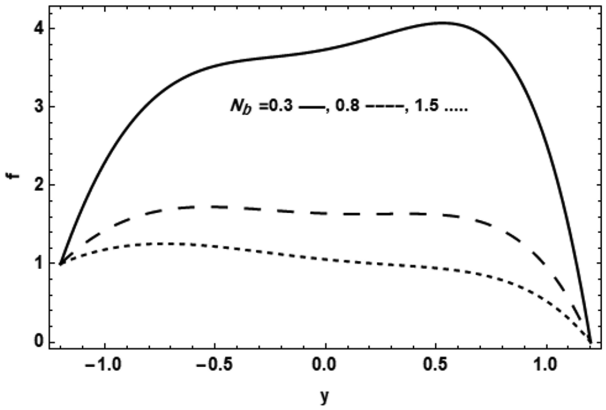

Fig. 10 — The concentration f for different values of N_b where $h=1.2$, $\partial p/\partial x=1$, $W_e=0.1$, $U_{HS}=3$, $\Omega=2$, $S=1.5$, $\omega=1.03$, $N_t=0.4$, $k=0.3$, $Ec=2$, $Pr=0.5$, $Sc=0.5$, $E_A=0.5$, $k_\alpha=0.8$, $n=2$

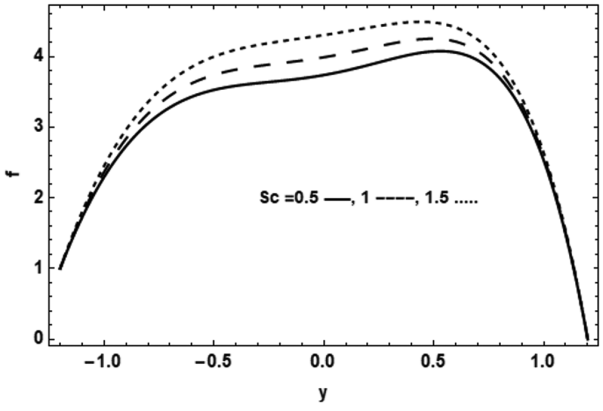

Fig. 11 — The concentration f for different values of Sc where $h=1.2$, $\partial p/\partial x=1$, $W_e=0.1$, $U_{HS}=3$, $\Omega=2$, $S=1.5$, $\omega=1.03$, $N_t=0.4$, $N_b=0.3$, $Ec=2$, $Pr=0.5$, $k=0.3$, $E_A=0.5$, $k_\alpha=0.8$, $n=2$

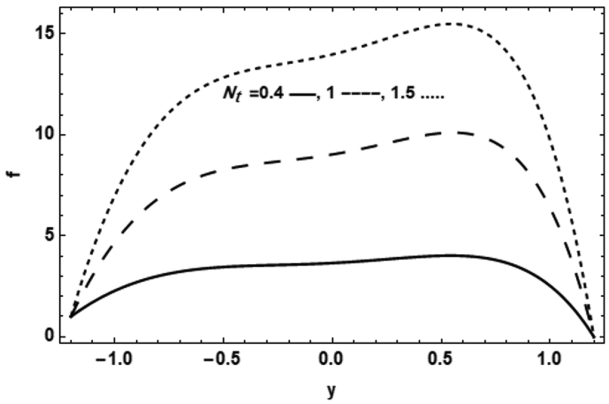

Fig. 12 — The concentration f for different values of N_t where $h=1.2$, $\partial p/\partial x=1$, $W_e=0.1$, $U_{HS}=3$, $\Omega=2$, $S=1.5$, $\omega=1.03$, $k=0.3$, $N_b=0.3$, $Ec=2$, $Pr=0.5$, $Sc=0.5$, $E_A=0.5$, $k_\alpha=0.8$, $n=2$

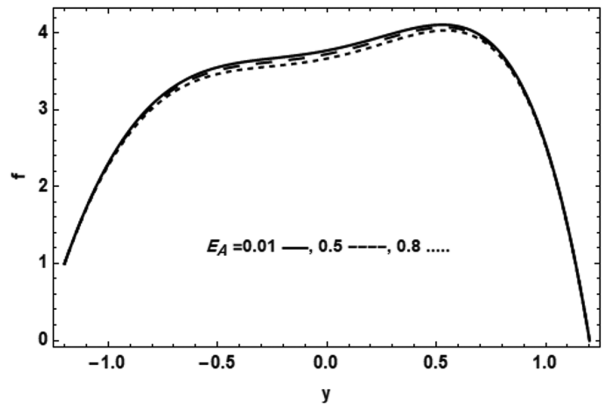

Fig. 13 — The concentration f for different values of E_A where $h=1.2$, $\partial p/\partial x=1$, $W_e=0.1$, $U_{HS}=3$, $\Omega=2$, $S=1.5$, $\omega=1.03$, $k=0.3$, $N_b=0.3$, $Ec=2$, $Pr=0.5$, $Sc=0.5$, $N_t=0.4$, $k_\alpha=0.8$, $n=2$

temperature distribution[18]. This, in turn, amplifies the concentration profile.

Fig. 13 illustrates that f increases with an increase in the Chemical reaction parameter k_α. While Fig. 14 illustrates that f decreases as the activation parameter E_A increase. The activation energy in physical chemistry refers to the minimum energy required to start a chemical reaction. The Arrhenius equation shows that activation energy and reaction rate are inversely related. In other words, as activation energy increases, reaction rate decreases, and vice versa. Therefore, the higher activation energy in

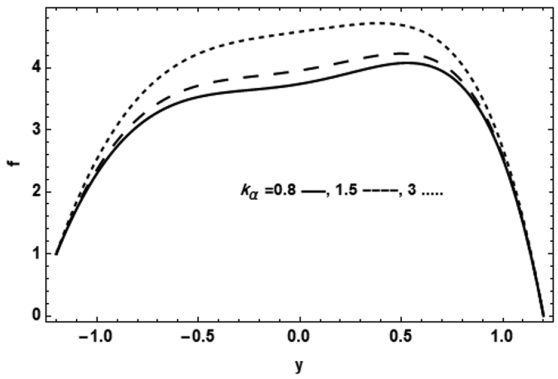

Fig. 14 — The concentration f for different values of k_α where $h=1.2$, $\partial p/\partial x=1$, $W_e=0.1$, $U_{HS}=3$, $\Omega=2$, $S=1.5$, $\omega=1.03$, $k=0.3$, $N_b=0.3$, $Ec=2$, $Pr=0.5$, $Sc=0.5$, $N_t=0.4$, $E_A=0.5$, $n=2$

Fig. 14 leads to the slower reaction rate shown in Fig. 13, as expected based on this relationship.

Conclusion

In the current paper, the peristaltic transport of unsteady incompressible non-Newtonian nanofluid inside a horizontal micro-channel is studied; the non-Newtonian is pseudoplastic fluid that obeys Williamson model, the flow is through a modified Darcy porous medium in the presence electroosmotic. The electro-osmotic phenomenon, and the effect of chemical reaction with activation energy are taken in consideration. The most main results of this study can be outlined and summarized as follows:

1. The product of (the strain rate) and (the relaxation time) is always constant and this constant is called Weissenberg number W_e, it is found that near the lower wall of the tube (hot wall) as W_e increases (the relaxation time) increases and (the strain rate) decreases, while vice versa occurs near the upper wall.
2. Weissenberg number W_e has a dual effect on the velocity profile as well as the temperature and concentration profiles. This is due to sparring between the domination of Plasticity and viscosity.
3. The study of the same model in case of Newtonian fluid can be obtained by putting $W_e=0$.
4. As the thickness of the EDL decrease (Ω increases), the concentration profile is not changed, on the other hand the net flow of the

charged particles decreases, which in turns reduces the temperature profile of the fluid.

5. According to Fick's law of diffusion; the temperature and concentration distributions should have opposite effects, however, it is found that the increment in the thermophoresis parameter increases both temperature and concentration distributions , this means that in case of horizontal tube, the nanoparticles are more concentrated and their flow from hot region to cold region is much better.
6. Moreover, by considering $\frac{T_0}{2} < T_1 < T_0$, the term of the activation energy is simplified by using Taylor expansion, and the system of the governing equations is ready to be solved by homotopy perturbation.

Nomenclature

	Roman Symbols	SI Units
a	The amplitude of the wave	m
A	Chemical reaction rate	mol/(m^3·s)
$\bar{c}$	The wave velocity	m s^{-1}
C	The nanoparticle concentration in the fixed and moving frames	particles/m³
D_B	Brownian diffusion coefficient	–
D_T	Thermophoretic diffusion coefficient	–
e	The electronic charge.	The elementary charge "e"
Ec	Eckert number	–
E_a	Activation energy	–
f	The dimensionless nanoparticle concentration	–
f_0	The nanoparticle concentration at $y = 0$	–
f_1	The nanoparticle concentration at $y = H$	–
$H(x)$	transverse vibration of the wall	–
k	Permeability constant	H (Henry)/m
K	Thermal conductivity	W m^{-1} K^{-1}
k_α	Dimensionless Chemical reaction parameter	–
k_B	Boltzmann constant	–
n	Fitted rate constant	s^{-}1
N_b	Brownian motion parameter	–
N_T	Thermophoresis parameter	–
N_0	Bulk volume concentration for positive or negative ions	mol/m³
P	The fluid pressure	Kg m^{-1}s^{-2}
Sc	Schmidt number	–
Pr	Prandtl number	–
T	The fluid temperature in the fixed and moving frames	K (Kelvin)
T_0	Temperature at $y=0$	K
T_{av}	Local absolute temperature	K
T_1	Temperature at $y = H$	K (Kelvin)
W_e	Weissenberg number	–
x	Axial coordinate	m
y	Transverse coordinate	m
z	The valence number of ions.	–
	Greek symbols	
Γ	is the time constant	–
θ	The dimensionless fluid temperature	–
ϕ	Electric potential for EDL (Zeta potential)	Volts (V)
ζ	Zeta potential at the upper wall	Volts (V)
U_{HS}	The dimensionless Helmholtz-Smoluchowski velocity	–
Ω	Electroosmotic parameter	–
ν_μ	Kinematic viscosity of fluid	m²/s
μ_0	Dynamic viscosity of fluid	(Pa·s) or N·s/m²
μ	apparent viscosity of fluid	(Pa·s) or N·s/m²
ρ_e	Density of the total ionic energy	Joules per cubic meter (J/m³).
ε	Electric permittivity	Farads per meter (F/m).
n^+	The number of density of cations	m^{-3}
n^-	The number of density of anions	m^{-3}
γ	Shear strain	–
λ	Wavelength	m
λ_α	The thickness of EDL (Debye length)	m
ρ_f	The density of the fluid	kg/m³
ρ_P	The density of the particle	kg/m³
$(\rho c)_f$	Heat capacity of the fluid	Joules per kelvin per kilogram (J/(K·kg)).
$(\rho c)_P$	Effective heat capacity of the nanoparticles material	Joules per kelvin per kilogram (J/(K·kg)).

References

1 Eldabe N T M, Hassan M A & Abou-Zeid M Y, Wall properties effect on the peristaltic motion of a coupled stress fluid with heat and mass transfer through a porous medium, *J Eng Mech*, 142 (2016) 4015102.

2 Sharma B K, Gandhi R, Abbas T & Bhatti M M, Magnetohydrodynamics hemodynamics hybrid nanofluid flow through inclined stenotic artery, *Appl Math Mech*, 44 (2023) 459.

3 Ram D, Bhandari D S, Tripathi D & Sharma K, Propagation of H1N1 virus through saliva movement in oesophagus: a mathematical model, *Eur Phys J Plus*, 137 (2022) 866.

4 Ram D, Bhandari D S, Sharma K & Tripathi D, Progression of blood-borne viruses through bloodstream: A comparative mathematical study, *Comput Meth Prog Biomed*, 232 (2023) 107425.

5 Abdelmoneim M, Eldabe N T, Abouzeid M Y & Ouaf M E, Both modified Darcy's law and couple stresses effects on electro-osmotic flow of non-Newtonian nanofluid with peristalsis, *Int J Appl Electromagn Mech*, 72 (2023) 1.

6 El-Dabe N T M, Abou-zeid M Y, Mohamed M A A & Abd-Elmoneim M M, Peristaltic mixed convection slip flow of a Bingham nanofluid through a non-Darcy porous medium in an inclined non-uniform duct with viscous dissipation and radiation, *J Appl Nonlinear Dyn*, 12 (2023) 231.

7 Ismael A M, Eldabe N T & El-Shabouri S M, Thermal micropolar and couple stresses effects on peristaltic flow of biviscosity nanofluid through a porous medium, *Sci Rep*, 12 (2022) 1.

8 Eldabe N T, Abou-zeid M Y, Abosaliem A, Elenna A & Hegazy N, Homotopy perturbation approach for Ohmic dissipation and mixed convection effects on non-Newtonian nanofluid flow between two co-axial tubes with peristalsis, *Int J Appl Electromagn Mech*, 67 (2021) 153

9 Hayat T, Iqbal R, Tanveer A & Alsaedi A, Mixed convective peristaltic transport of Carreau-Yasuda nanofluid in a tapered asymmetric channel, *J Mol Liq*, 223 (2016) 1100.

10 Mishra N K, Sharma B K, Sharma P, Muhammad T & Pérez L M, Entropy generation optimization of cilia regulated MHD ternary hybrid Jeffery nanofluid with Arrhenius activation energy and induced magnetic field, *Sci Rep*, 13 (2023) 14483.

11 Eldabe N T M, Abou-Zeid M Y, Ouaf M E, Mustafa D R & Mohammed Y M, Cattaneo–Christov heat flux effect on MHD peristaltic transport of Bingham Al_2O_3 nanofluid through a non–Darcy porous medium, *Int J Appl Electromagn Mech*, 68 (2022) 59.

12 Eldabe N T, Moatimid G M, Abouzeid M Y, El Shekhipy A A & Abdallah N F, A semianalytical technique for MHD peristalsis of pseudoplastic nanofluid with temperature-dependent viscosity: Application in drug delivery system, *Heat Transfer Res*, 49 (2020) 424.

13 Eldabe N T, El Shaboury S M, El Arabawy H A, Abou-zeid M Y & Abuiyada A, Wall properties and Joule heating effects on MHD peristaltic transport of Bingham non-Newtonian nanofluid, *Int J Appl Electromagn Mech*, 69 (2022) 87.

14 Abou-zeid MY & Ouaf M E, Effect of thermophoresis and mixed convection on Carreau fluid flow with gold nanoparticles, *Egypt J Chem*, 66 (2023) 2191.

15 Mansour H M & Abou-zeid M Y, Heat and mass transfer effect on non-Newtonian fluid flow in a non-uniform vertical tube with peristalsis, *J Adv Res Fluid Mech Therm Sci*, 61 (2019) 44.

16 Williamson R V, The flow of pseudoplastic materials, *Indian Eng Chem*, 21 (1929) 1108.

17 Nadeem S & Akram S, Peristaltic flow of a Williamson fluid in an asymmetric channel, *Commun Nonlinear Sci Numer Simul*, 15 (2010) 1705.

18 Eldabe N, Abo-Seida O M, Abo-Seliem A A S, Elshekhipy A A & Hegazy N, Magnetohydrodynamic peristaltic flow of Williamson nanofluid with heat and mass transfer through a non-Darcy porous medium, *Microsyst Technol*, 24 (2018) 3751.

19 Rashid M, Ansar K & Nadeem S, Effects of induced magnetic field for peristaltic flow of Williamson fluid in a curved channel, *Phys A Stat Mech Appl*, 553 (2020) 123979.

20 Abou-zeid M Y & Ouaf M E, Hall currents effect on squeezing flow of non-Newtonian nanofluid through a porous medium between two parallel plates, *Case Stud Therm Eng*, 28 (2021) 101362.

21 Eldabe N T, Moatimid G M, Abouzeid M, El-Shekhipy A A & Abdallah N F, Instantaneous thermal-diffusion and diffusion-thermo effects on carreau nanofluid flow over a stretching porous sheet, *J Adv Res Fluid Mech Therm Sci*, 72 (2020) 142

22 Eldabe N T, Rizkalla R R, Abouzeid M Y & Ayad V M, Thermal diffusion and diffusion thermo effects of Eyring-Powell nanofluid flow with gyrotactic microorganisms through the boundary layer, *Heat Transfer Res*, 49 (2020) 383.

23 Eldabe N T, Moatimid G M, Abouzeid M, Elshekhipy A A & Abdallah N F, Semi-analytical treatment of Hall current effect on peristaltic flow of Jeffery nanofluid, *Int J Appl Electromagn Mech*, 67 (2021) 47.

24 Abou-Zeid M Y, Homotopy perturbation method for couple stresses effect on MHD peristaltic flow of a non-Newtonian nanofluid, *Microsyst Technol*, 24 (2018) 4839.

25 El-Dabe N T M, Abou-Zeid M Y, Mohamed M A A & Abd-Elmoneim M M, MHD peristaltic flow of non-Newtonian power-law nanofluid through a non-Darcy porous medium inside a non-uniform inclined channel, *Arch Appl Mech*, 91 (2021) 1067.

26 El-dabe N T, Abou-zeid M Y, Mohamed M A & Maged M, Peristaltic flow of Herschel Bulkley nanofluid through a non-Darcy porous medium with heat transfer under slip condition, *Int J Appl Electromagn Mech*, 66 (2021) 649.

27 Abou-Zeid M Y, Homotopy perturbation method to gliding motion of bacteria on a layer of power-law nanoslime with heat transfer, *J Comput Theor Nanosci*, 12 (2015) 3605.

28 Eldabe N T, El Shabouri S M, Salama T N & Ismael A M, Ohmic and viscous dissipation effects on micropolar non-Newtonian nanofluid Al_2O_3 flow through a non-Darcy porous media, *Int J Appl Electromagn Mech*, 68 (2022) 209.

29 Mostafa Y, El-Dabe N, Abou-Zeid M, Oauf M & Mostapha D, Peristaltic transport of Carreau coupled stress nanofluid with Cattaneo-Christov heat flux model inside a symmetric channel, *J Adv Res Fluid Mech Therm Sci*, 98 (2022) 1.

30 Sharma B K, Kumawat C, Khanduri U & Mekheimer K S, Numerical investigation of the entropy generation analysis for radiative MHD power-law fluid flow of blood through a curved artery with Hall effect, *Waves RCM*, (2023) 1.

31 Eldabe N T, Abou-zeid M Y, Seliem A S A, Elenna A A & Hegazy N, Thermal diffusion and diffusion thermo effects on magnetohydrodynamics transport of non-Newtonian nanofluid through a porous media between two wavy co-axial tubes, *IEEE Trans Plasma Sci*, 50 (2022) 1282.

32 Abuiyada A J, Eldabe N T, Abou-zeid M Y & El Shaboury S M, Effects of thermal diffusion and diffusion thermo on a chemically reacting MHD peristaltic transport of Bingham

plastic nanofluid, *J Adv Res Fluid Mech Therm Sci*, 98 (2022) 24.
33 Sharma K & Kumar S, Impacts of low oscillating magnetic field on ferrofluid flow over upward/downward moving rotating disk with effects of nanoparticle diameter and nanolayer, *J Magn Magn Mater*, 575 (2023) 170720.
34 Alizadeh A, Hsu W, Wang M & Daiguji H, Electroosmotic flow: From microfluidics to nanofluidics, *Electrophoresis*, 42 (2021) 834.
35 Suriyage N U, Ghantasala M K, Iovenitti P & Harvey E C, Fabrication, measurement, and modeling of electro-osmotic flow in micromachined polymer microchannels, *Biomed Nanotechnol*, 5275 (2004) 149.
36 Noreen S, Waheed S, Lu D C & Hussanan A, Heat measures in performance of electro-osmotic flow of Williamson fluid in micro-channel, *Alex Eng J*, 59 (2020) 4081.
37 Prakash J & Tripathi D, Electroosmotic flow of Williamson ionic nanoliquids in a tapered microfluidic channel in presence of thermal radiation and peristalsis, *J Mol Liq*, 256 (2018) 352.
38 Moatimid G M, Mohamed M A A, Hassan M A & El-Dakdoky E M M, Electro-osmotic flow and heat transfer of a non-Newtonian nanofluid under the influence of peristalsis, *Pramana*, 92 (2019) 1.
39 El-Dabe N T M, Moatimid G M, Hassan M A & Godh W A, Electro-osmotic and Hall Current Effects on the Nanofluid Flow through Porous Medium with Wall Properties, *Int J Appl Eng Res*, 14 (2019) 3552.
40 Rafiq M, Sajid M, Alhazmi S E, Khan M I & El-Zahar E R, MHD electroosmotic peristaltic flow of Jeffrey nanofluid with slip conditions and chemical reaction, *Alex Eng J*, 61 (2022) 9977.
41 Ellahi R, Zeeshan A, Hussain F & Asadollahi A, Peristaltic blood flow of couple stress fluid suspended with nanoparticles under the influence of chemical reaction and activation energy, *Symmetry*, 11 (2019) 276.
42 Ibrahim M, Abdallah N & Abouzeid M, Activation energy and chemical reaction effects on MHD Bingham nanofluid flow through a non-Darcy porous media, *Egypt J Chem*, 65 (2022) 715.
43 Zhao C, Wang Q & Zeng M, Perturbation solutions for the nonlinear Poisson–Boltzmann equation with a high-order-accuracy Debye–Hückel approximation, *Z Angew Math Phys*, 71 (2020) 1.
44 Tripathi D, Bhushan S & Bég O A, Analytical study of electro-osmosis modulated capillary peristaltic hemodynamics, *J Mech Med Biol*, 17 (2017) 1750052.
45 Akbar N S, Nadeem S, Lee C, Khan Z H & Haq R U, Numerical study of Williamson nano fluid flow in an asymmetric channel, *Results Phys*, 3 (2013) 161.
46 Poole R J, The Deborah and Weissenberg numbers, *Rheol Bull*, 53 (2012) 32.
47 Chaube M K, Yadav A, Tripathi D & Bég O A, Electroosmotic flow of biorheological micropolar fluids through microfluidic channels, *Korea-Aust Rheol J*, 30 (2018) 89.
48 Ahmed O S, Eldabe N T, Abou-Zeid M Y, El-Kalaawy O H & Moawad S M, Numerical treatment and global error estimation for thermal electro-osmosis effect on non-Newtonian nanofluid flow with time periodic variations, *Sci Rep*, 13 (2023) 14788.
49 Eldabe N T & Abou-zeid M Y, Magnetohydrodynamic peristaltic flow with heat and mass transfer of micropolar biviscosity fluid through a porous medium between two co-axial tubes, *Arab J Sci Eng*, 39 (2014) 5045.
50 Mohamed M A A & Abou-zeid M Y, MHD peristaltic flow of micropolar Casson nanofluid through a porous medium between two co-axial tubes, *J Porous Media*, 22 (2019) 1079.
51 Abou-zeid M Y & Mohamed M A A, Homotopy perturbation method for creeping flow of non-Newtonian power-law nanofluid in a nonuniform inclined channel with peristalsis, *Z Naturforsch A*, 72 (2017) 899.
52 Abou-Zeid M Y, Shaaban A A & Alnour M Y, Numerical treatment and global error estimation of natural convective effects on gliding motion of bacteria on a power-law nanoslime through a non-Darcy porous medium, *J Porous Media*, 18 (2015) 1091.
53 Subbarayudu K, Suneetha S, Wahidunnisa L & Reddy P B A, Impact of chemical reaction on radiating Falkner-Skan flow over a wedge moving in a Carreau nanofluid with convective condition, *Int J Tech Innov Mod Eng Sci*, 4 (2018) 1353.
54 Abou-Zeid M, Effects of thermal-diffusion and viscous dissipation on peristaltic flow of micropolar non-Newtonian nanofluid: application of homotopy perturbation method, *Results Phys*, 6 (2016) 481.
55 Sheikholeslami M & Ganji D D, Unsteady nanofluid flow and heat transfer in presence of magnetic field considering thermal radiation, *J Braz Soc Mech Sci Eng*, 37 (2015) 895.
56 Hayat T, Khan A A, Bibi F & Farooq S, Activation energy and non-Darcy resistance in magneto peristalsis of Jeffrey material, *J Phys Chem Solids*, 129 (2019) 155.
57 Khanduri U, Sharma B K, Sharma M, Mishra N K & Saleem N, Sensitivity analysis of electroosmotic magnetohydrodynamics fluid flow through the curved stenosis artery with thrombosis by response surface optimization, *Alex Eng J*, 75 (2023) 1.
58 Sharma B K, Sharma P, Mishra N K, Noeiaghdam S & Fernandez-Gamiz U, Bayesian regularization networks for micropolar ternary hybrid nanofluid flow of blood with homogeneous and heterogeneous reactions: Entropy generation optimization, *Alex Eng J*, 77 (2023) 127.
59 Gandhi R, Sharma B K, Mishra N K & Al-Mdallal Q M, Computer simulations of EMHD Casson nanofluid flow of blood through an irregular stenotic permeable artery: application of Koo-Kleinstreuer-Li correlations, *Nanomaterials*, 13 (2023) 652.
60 Sharma P K, Sharma B K, Mishra N K & Rajesh H, Impact of Arrhenius activation energy on MHD nanofluid flow past a stretching sheet with exponential heat source: A modified Buongiorno's model approach, *Int J Mod Phys B*, 37 (2023) 2350284.
61 Sharma K, Animasaun I L & Al-Mdallal Q M, Scrutinization of Ferrohydrodynamic through pores on the surface of disk experiencing rotation: Effects of FHD interaction, thermal radiation, and internal heat source, *Arab J Sci Eng*, (2023). https://doi.org/10.1007/s13369-023-07853-2